ACS Sustainable Chemistry & Engineering

Research Article

pubs.acs.org/journal/ascecg

Bioderived "Green" Composite from Soy Protein and Eggshell Nanopowder

M. M. Rahman,[†] A. N. Netravali,*[,†] B. J. Tiimob,[‡] and V. K. Rangari[‡]

[†]Department of Fiber Science and Apparel Design, Cornell University, 37 Forest Home Drive, Ithaca, New York 14850, United States

[‡]Department of Material Science and Engineering, Tuskegee University, 100 Chappie James Center, Tuskegee, Alabama 36088, United States

Supporting Information

ABSTRACT: A bioderived and ecofriendly hybrid nanocomposite was developed from soy protein and eggshell nanopowder (ESNP). ESNP was synthesized via size reduction of chicken eggshells using ball milling followed by a sonochemical process. Transmission electron microscopy and X-ray diffraction (XRD) studies revealed calcite particles in ESNP with sizes ranging between 20 and 40 nm. A trace of protein with the as-synthesized ESNP was detected through X-ray photon spectroscopy (XPS) observation. Dispersion of ESNP in water was achieved by using a polyanionic dispersant via an adsorption mechanism. Green nanocomposites were developed from soy protein isolate (SPI) and dispersed ESNP using glycerol, a natural plasticizer, by a solution casting process. Significant improvements in Young's modulus, tensile strength, and thermal stability of SPI nanocomposite sheets were achieved as a result of incorporation of well-dispersed ESNP. The developed ESNP-incorporated SPI nanocomposite would be inexpensive and useful to fabricate sustainable "green" composite structures.

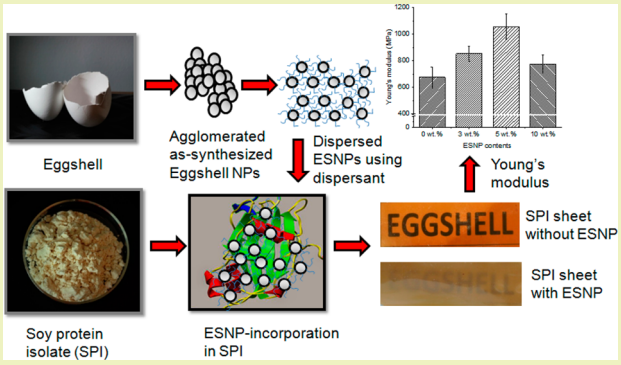

KEYWORDS: *Nanocomposite, Eggshell, Soy protein, Calcium carbonate, Green composite*

INTRODUCTION

Development of environmently friendly and biodegradable "green" materials from low-cost or freely available natural and renewable resources such as agricultural and food waste products has received considerable attention due to worldwide ecological awareness and economic concerns. If not utilized, most of these waste products end up in landfills. Proteins, one of the naturally occurring macromolecules, offer a wide range of potential functional properties as a biobased resin for composite structures through the formation of numerous intermolecular bonds due to the presence of polar amino acids.[1−4] Soy protein, a byproduct of soybean oil extraction, has been considered as one of the major biobased resins that can be processed into sustainable composites using modifiers such as plasticizers, cross-linkers, and reinforcing agents.[5−8] Soy protein is commercially available in three different varieties: defatted soy flour (SF) with about 53−55% protein, soy protein concentrate (SPC) with about 70% protein, and soy protein isolate (SPI) with about 90% protein. All have been used as resins in composites after some modifications.[1,2,4,6] There are two major fractions in soy protein, 7S (30% of total soy protein) and 11S (40% of total soy protein), which contain various polar functional groups, such as carboxyl, amine, and hydroxyl groups. These groups are capable of chemically reacting to form cross-links and thus improve the mechanical and physical properties of the protein.

Chicken eggshell, a bioceramic composite, consists of inorganic minerals, i.e., calcium carbonate (94%), calcium phosphate (1%), magnesium carbonate (1%), in an organic matrix (4%) consisting of collagen, sulfated polysaccharides, and other polypeptides.[9] About 11% of the total weight of a chicken egg is egg shell that is considered as waste residue in food-processing and manufacturing industries.[10] More than 45 million kg of eggshell wastes are disposed of every year without further processing in the United States.[11] The unique chemical compositions and abundance of the eggshell makes it a viable and free source of biobased calcium carbonate. As of now, the utilization of eggshell calcium carbonate has been investigated as additive for animal feed,[12] human nutrition,[13] coating pigments for inkjet printing paper,[11] natural absorbent of heavy metals,[14] dye-effluents remover,[15] bone substitute,[16] and biofiller for polymer-based composites.[17−19]

The effects of fillers on the functional properties of the composite materials depend on shape, size, surface characteristics, and degree of dispersion. Previously, it has been reported that composites with nanoparticles showed better properties than composites with microparticles of the same filler.[20] Higher specific surface area of nanoparticles as compared to micro-

Received: May 14, 2014
Revised: August 29, 2014
Published: September 2, 2014

particles provides a higher desirable interface for stress transfer and lower stress concentration factors in composites. However, due to high specific surface area and energy, nanoparticles induce undesirable van der Waals and electrostatic forces between each other, mostly resulting in excessive agglomerations.[21] These agglomerations produce unwanted stress concentration points in the nanocomposites and lead to the deterioration of the mechanical properties of their composites.[22] As a result, uniform and stable dispersion is highly desired to effectively utilize the potential of nanoparticles in composites. In past decades, researchers have been successful in tailoring various resin properties, particularly stiffness and toughness, by incorporating calcium carbonate nanoparticles to fabricate advanced inorganic particulate-filled polymer-based nanocomposites.[23−26] It is expected that eggshell (biobased calcium carbonate) nanopowder can be utilized as biofillers for protein-based green composites to enhance stiffness and strength as electrostatic interaction between acidic amino acids and calcium ions takes place when calcium ions are added to soy protein.[24]

Primarily inspired from the nature of biominerals of inorganic crystals in shell or bone protein, eggshell nanopowder (ESNP) was incorporated in soy protein as nanofiller to develop a new "fully sustainable green nanocomposite" that will have significant environmental benefits, good functionality, and biodegradability. In this study, ESNP was synthesized via ball milling and sonochemical processes from waste eggshell. ESNP was dispersed in water using a suitable polyanionic surfactant. Bioderived and ecofriendly nanocomposites were prepared using SPI and dispersed ESNP by a solution casting process. A detailed investigation on the characterization of ESNP and SPI-ESNP nanocomposites has been reported here.

EXPERIMENTAL SECTION

Materials. SPI powder was obtained from Archer Daniels Midland Co., Decatur, IL. Raw white eggshells were collected from American Dehydrated Foods, Inc., Springfield, MO. Analytical grade sodium hydroxide (NaOH) pellets, glycerol (≥98% purity), sodium polyacrylate (average molecular weight, $M_w \sim 5100$), ethanol (≥99.5% purity, absolute), and polypropylene glycol (average molecular weight, $M_n \sim 425$) were purchased from Sigma-Aldrich Chemical Co., Allentown, PA.

Preparation of Eggshell Nanopowder (ESNP). ESNP was synthesized via a top-down approach from the eggshell. The raw eggshell was boiled at 100 °C in an electric cooker (Hamilton Beach, Model: 33157) for 6 h and ground in a Waring commercial blender (Model: 51BL30) at a high speed for 10 min to separate the eggshell membrane from the eggshell. Organic materials contained in the eggshell membrane became denatured to release the particles for separation. Heavier eggshell powder mostly settled at the bottom and was collected and thoroughly washed with deionized (DI) water and then with pure ethanol. Finally, it was air-dried for 24 h at room temperature, and eggshell powder with an average particle size of 20−40 μm was obtained. In the ball milling process, 5 g of eggshell powder mixed with 10 mL of polypropylene glycol (PPG) was wet milled using 8 steel balls (~6 mm diameter) in a Spex Sample prep 8000D mill for 10 h. The PPG was used as a process control agent to further remove contamination during ball milling. After wet ball milling, the mixture was added to ethanol and washed by centrifuging four times for 5 min at 15,000 rpm (Allegra 64R, Beckman Coulter). In this process, the size was reduced to less than 20 μm. Then, the eggshell powder was mixed with 400 mL 0.01 M CH_3COOH by a magnetic stirrer at 1200 rpm for 30 min. This suspension was subjected to ultrasonication for 5 h using ultrasound irradiation (Sonics vibra cell ultrasound, Model VCX 1500) at 50% amplitude and 25 °C to further reduce the size of the eggshell particles. After ultrasonication, the suspension was centrifuged at 15,000 rpm in a Beckman Coulter centrifuge (Model ALLEGRA-64R). The supernatant was separated, and the remaining powder, designated as ESNP, was dried in a vacuum oven for 24 h.

Dispersion of Eggshell Nanopowder in Water. ESNP was dispersed in DI water at various contents of 3, 5, and 10 wt % of SPI resin. First, 3−10 wt % of ESNP was mixed with DI water, and the suspension was stirred by magnetic stirrer for 1 h to wet the particles completely. Then, the mixture was ultrasonicated (Branson Ultrasonics, Model 2510, Mumbai, India) at 60 °C for about 1 h to break up the aggregated ESNP in aqueous solution. Sodium polyacrylate (PAANa) as anionic dispersant was added to the sonicated suspension at 10 wt % of ESNP contents. The mixture was stirred using a magnetic stirrer for about 15 min at room temperature.

Preparation of Soy Protein-Based Nanocomposites. SPI was added to 3, 5, and 10 wt % ESNP colloidal suspensions, and DI water was added to make a ratio of 1:10 (SPI-ESNP:water) on a weight basis. Sheets made of SPI itself were too brittle to handle. Glycerol was added as plasticizer at 10 wt % of SPI to overcome the brittleness. The pH of the solution was adjusted to 10.5 ± 0.2 using a 1 M NaOH solution. After homogenizing the mixtures for 20 min, the solution was stirred further for 30 min at 80 °C. The solution was dried on Teflon-coated glass plate for 24 h in an air-circulated oven maintaining 40 °C. Finally, dried SPI-ESNP nanocomposite sheets were cured using a Carver hydraulic hot press at 140 °C for 20 min under a pressure of 2.5 MPa. The specimens were conditioned at 65% RH and 21 °C before all testing. SPI sheets incorporated with 3, 5, and 10 wt % ESNP will be designated as SPI-ESNP3, SPI-ESNP5, and SPI-ESNP10, respectively.

Characterizations. X-ray diffraction (XRD) patterns of as-synthesized ESNP were recorded on an X-ray diffractometer (Scintag theta−theta) equipped with Cu Kα_1 radiation (λ = 0.154 nm) at 40 kV and 40 mA. Data were collected from 20° to 50° Bragg angles (2θ) at a scan rate of 3 deg/min and a step interval of 0.02°. X-ray photoelectron spectroscopy (XPS) or electron spectroscopy for chemical analysis (ESCA) was conducted to analyze the as-synthesized ESNP surfaces quantitatively and qualitatively to a depth of about 10 nm. The elemental composition was determined by XPS (model, SSX-100; manufacturer, Surface Science Instruments) equipped with aluminum Kα X-rays, and all binding energies were referenced to the carbon C 1s energy peak at 284.63 eV. Photoemission electrons were collected at a 55° emission angle, and the hemispherical analyzer used a 150 V pass energy for survey scans and 50 V pass energy for high resolution scans. Attenuated total reflection-Fourier transform infrared (ATR-FTIR) spectra were collected using a Bruker Vertex 80 V FTIR spectrometer. All spectra were an average of 256 scans recorded from 4000 to 600 cm^{-1} wave numbers at a resolution of 2 cm^{-1}. High resolution transmission electron microscopy (HRTEM) images of ESNP were obtained using a JEOL-2010 transmission electron microscope (TEM). The samples were dispersed in ethanol using ultrasonication for 5 min at room temperature and placed on a copper grid; they were evaporated prior to observation.

The dispersion states of ESNP in SPI sheets were examined by optical microscopy (OM). Zeta (ζ) potential of calcium carbonate aqueous dispersions in the presence and absence of the anionic dispersant (PAANa) were measured at ambient temperature using Malvern Zetasizer Nano ZS90 according to the Smoluchowski's equation.[27] Particle size distributions of ESNP in water in the presence and absence of anionic dispersant were determined by dynamic light scattering (Zetasizer Nano ZS90, Malvern Instruments Ltd., Malvern, UK) at a wavelength of 633 nm. Suspension was prepared by dispersing 10 mg ESNP in 20 mL DI water using a magnetic stirrer followed by ultrasonication for 30 min. Anionic dispersant (PAANa) was dissolved on the basis of 10 wt % of ESNP.

Moisture content (MC) of SPI composite sheets was measured according to a method described by Rhim et al.[28] The specimens were weighed (W_1), subsequently dried in an air-circulating oven at 105 °C for 24 h, and reweighed (W_2) to determine MC values using eq 1

$$\text{MC}\ (\%) = \left(1 - \frac{W_2}{W_1}\right)100 \quad (1)$$

Mechanical properties of SPI composite sheets were determined according to ASTM D880-02 with an Instron universal tensile testing machine. Young's modulus, tensile strength, and fracture strain were measured from the tests. Sheets with dimensions of 10 mm × 60 mm were tested at the strain rate of 1 min^{-1} and a gauge length of 30 mm after conditioning. A minimum of 10 specimens were tested for each composition. Thermal degradation behavior of resin sheets was investigated using thermogravimetric analysis, TGA (TGA-2050, TA Instruments, Inc., DE). Specimens weighing (approximately 10 mg) were scanned from 30 to 1000 °C at a heating rate of 10 °C/min under a flow of 60 mL/min nitrogen gas.

Transmission electron microscopy (TEM) images of SPI resin sheets were obtained using FEI Tecnai T12 TEM to show the dispersion in the resins. The specimens were cut into very thin sections using Leica EM UC7 ultramicrotome and placed on a copper grid prior to observation. Fracture surface analysis was carried out using a Tescan Mira3 field emission scanning electron microscope (FESEM) at 7 kV accelerating voltage. Specimen surfaces were sputter coated with a thin layer of gold to prevent charging. Energy dispersive spectroscopy (EDS) was performed using a Bruker energy dispersive spectrometer equipped with Tescan Mira3 FESEM to perform point and mapping analysis of Ca elements in fracture surfaces to confirm the presence of ESNP. XRD patterns of resin and composite sheets were collected from 5° to 35° Bragg angles (2θ) at a scan rate of 3 deg/min and a step interval of 0.02° with similar equipment used for the as-synthesized ESNP characterization.

Statistical evaluations were carried out by analysis of variance (ANOVA) followed by multiple comparison tests using Tukey–Kramer's HSD at a 95% confidence level. All analyses were performed using JMP statistical software (SAS Institute, Cary, NC).

RESULTS AND DISCUSSION

Characteristics of ESNP. Figure 1 shows the representative XRD pattern of the as-synthesized ESNP. Characteristic

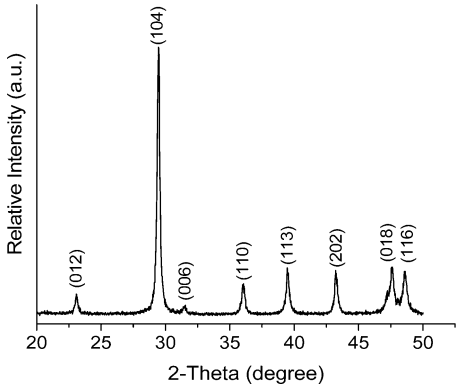

Figure 1. XRD pattern of as-synthesized eggshell nanopowder (ESNP).

diffraction peaks appeared with diffraction angles at 23.10°, 29.46°, 36.05°, 39.46°, 43.22°, 47.58°, and 48.56°. These diffraction data revealed that the as-synthesized ESNP contained the thermo-dynamically most stable calcite crystalline phase that is matched closely with those of PDF2 standard card (00-005-0586) patterns (Mineral Powder Diffraction File Data Book ICDD No. 5-586).

The crystallite size (τ_{hkl}) of ESNP in the direction perpendicular to the crystal face of (hkl) was estimated from the obtained diffraction peaks using the scherrer equation as follows[29]

$$\tau_{hkl} = \frac{k\lambda}{\beta_{1/2}\cos\theta} \quad (2)$$

where λ is the X-ray wavelength (0.154 nm), k is a constant with a value of 0.9,[24] $\beta_{1/2}$ is the full width at half-maximum intensity of diffraction peaks corresponding to the (hkl) lattice plane, and θ is the diffraction angle. Also, interplanar distances (d-spacing or d_{hkl}) in different crystal directions of ESNP were calculated from Bragg's equation as follows[29]

$$d_{hkl} = \frac{\lambda}{2\sin\left(\frac{\pi\theta}{180}\right)} \quad (3)$$

Table 1 shows the calculated values of crystal sizes and d-spacing in ESNP. The sizes of the calcite crystals in ESNP were found to be in the range of 21–35 nm, and interplanar distances were in the range of 0.19–0.38 nm.

Figure 2 shows the XPS spectrum of ESNP. It is shown in the figure that the as-synthesized ESNP contains calcium,

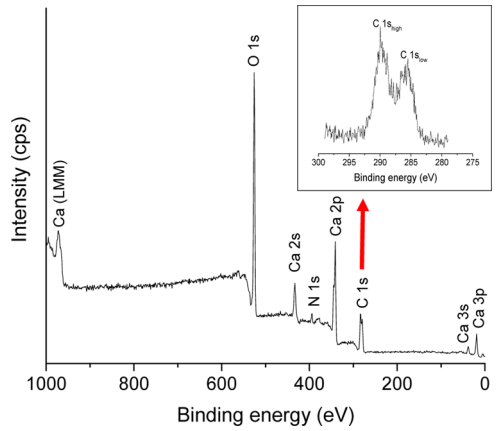

Figure 2. XPS spectrum of as-synthesized eggshell nanopowder (ESNP).

carbon, and oxygen elements with a trace amount of the nitrogen element. Also, the carbon C 1s spectrum has peaks at two binding energies: one at about 285 eV and the other at about 290 eV. A higher carbon concentration on the ESNP surfaces was observed at the higher binding energy peak (290 eV) representing the carbon associated with carbonate.[23] The presence of a carbon peak at a lower binding energy and a nitrogen peak might be an indication of the presence of organic matter, i.e., protein in ESNP from eggshell membranes.

Table 2 gives the quantitative measurements from the XPS analysis. As shown in Table 2, the presence of nitrogen was not significant as compared to other elements indicating that the

Table 1. Crystal Size and *d*-spacing of As-Synthesized ESNP

crystal face (hkl)	(012)	(104)	(110)	(113)	(202)	(018)	(116)
crystal size (nm)	32.5	34.1	30.8	33.3	34.9	21.2	27.2
d-spacing (nm)	0.385	0.303	0.249	0.228	0.209	0.191	0.187

Table 2. XPS Results of Eggshell Nanopowder (ESNP)

elements	Ca 2p	C $1s_{high}$	C $1s_{low}$	N 1s	O 1s
binding energy (eV)	347	290	285	400	532
percentages (%)	13.22	19.03	16.20	2.24	49.31

protein content was very low. This is expected because of the milling and other chemical processes involved in obtaining ESNP.

ATR-FTIR spectrum of ESNP (Figure S1, Supporting Information) showed typical characteristic absorption peaks at 713, 874, and 1396 cm^{-1} wavenumbers that can be assigned to in-plane bending, out-of-plane bending, and asymmetric stretching modes of CO_3^{2-}, respectively, associated with calcite. These observations are in good agreement with the results of XRD analysis. Also, a small peak at 1794 cm^{-1} can be assigned to the combination vibrations of C═O stretching and −NH− in-plane bending due to very small amounts of organic materials.

Figure 3 shows TEM micrographs of as-synthesized ESNP that reveal the highly agglomerated nature of the nanopowder.

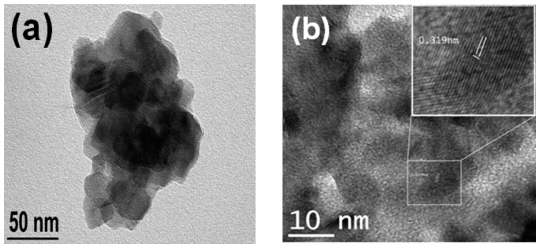

Figure 3. TEM images of as-synthesized eggshell nanopowder (ESNP).

The size distribution of the nanopowder was in the range of 20−40 nm. The sizes of the crystalline grains obtained from the TEM analysis were in close agreement with the crystal size calculated from the XRD studies. As shown in Figure 3(a), the nanopowder had an irregular combination of rhombohedral and quasi-spherical shapes. Figure 3(b) shows the ordered crystal lattice fringes in different crystal directions. Also, an interplanar distance of about 0.319 nm has been measured from the TEM image that is very close to the interplanar distance (104) plane of the calcite crystal (0.303 nm) as calculated from the Bragg equation. Overall, TEM and XRD analyses suggest high level crystallinity of as-synthesized ESNP.

Typical TGA and DTGA thermograms of as-synthesized ESNP (Figure S2, Supporting Information) indicated that the weight loss of ESNP was below 3.5% until the temperature reached 550 °C. This loss is related to release of any physisorbed water and eggshell membrane proteins. The degradation onset and maximum degradation temperature were obtained at 715 and 770 °C, respectively. Calcinations were observed between 600 and 850 °C with a weight loss of 45% resulting from phase change due to decomposition of calcium carbonate ($CaCO_3$) to calcium oxide (CaO) and carbon dioxide (CO_2). The CaO phase was found when eggshell was calcined at 900 °C.

All of these characterizations of as-synthesized ESNP, discussed above, indicate that it can be used as nanofiller in biobased resin to improve the properties of composites. Because of the protein layer on the surface, the nanoparticle/resin bonding could be expected to be good, resulting in better nanocomposite properties.

Dispersion of ESNP in Water. The dispersion state of ESNP in SPI sheets obtained by various dispersion processes was observed through optical microscopy (Figure S3, Supporting Information). The dispersion obtained by high speed mechanical mixing for 1 h of as-synthesized ESNP in SPI resin solution showed a significant amount of agglomeration (Figure S3-a, Supporting Information). A comparatively improved dispersion of ESNP with less agglomeration in nanocomposites was obtained by a combined dispersion of mechanical stirring for 1 h and sonication for 1 h (Figure S3-b, Supporting Information). However, a good dispersion of ESNP for the water-based approach was achieved by using an optimum amount of dispersant or surfactant after combined dispersion of mechanical stirring and sonication (Figure S3-c, Supporting Information). According to the Derjaguin, Landau, Verwey, and Overbeek (DLVO) theory, interaction between nanoparticles in an aqueous dispersion is characterized by two opposite interactions: van der Waals attraction and electrostatic repulsion.[30,31] The electrostatic repulsive interaction can be controlled by adding ionic dispersant. In this study, anionic dispersant "PAANa" was chosen for its exceptional dispersion stability for calcium carbonate.[32,33] Cationic surfactants were not chosen as they have been found to flocculate calcium carbonate.[34] The adsorption mechanism of PAANa onto ESNP involves dissolution of sodium in water and attachment of a negative hairy layer of acrylate ion (PAA^-) onto the surface of ESNP (Ca^+).[35] Increased negative charges of ESNP thus produce an increase in electrostatic barrier or repulsions that prevent the approach of another surface-modified ESNP with the same charges and hence lead to better and stable dispersion in water. However, a minimum loading of PAANa was determined to avoid the negative effect by an excessive amount of surfactant in sheets along with good dispersion in SPI resin. Figure 4 shows the value of zeta (ζ) potential of ESNP in water

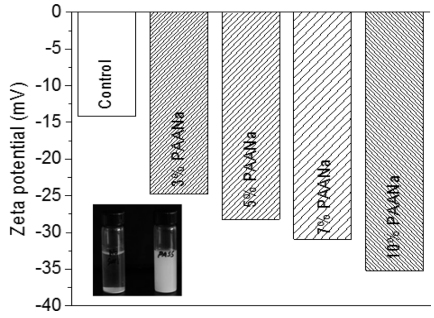

Figure 4. Zeta (ζ) potential of ESNP in water as a function of PAANa loading. Photographic image of the dispersion stability of ESNP alone and ESNP with PAANa is shown inset.

as a function of PAANa. ESNP in water without PAANa showed the ζ-potential value of −14 mV, whereas 7 and 10 wt % loading of PAANa increased the value to −30 mV and −35 mV, respectively. As discussed, an increase in magnitude of the surface charge leads to more stable and good aqueous dispersions. Generally, particles with ζ-potential values greater than ±30 mV are considered moderately stable and less than ±30 mV is unstable in a colloidal system.[36] The inset of Figure 4 shows a photographic image of the dispersion stability of ESNP alone and ESNP with PAANa in water after 1 h. As shown in Figure 4, aqueous dispersion of ESNP with PAANa

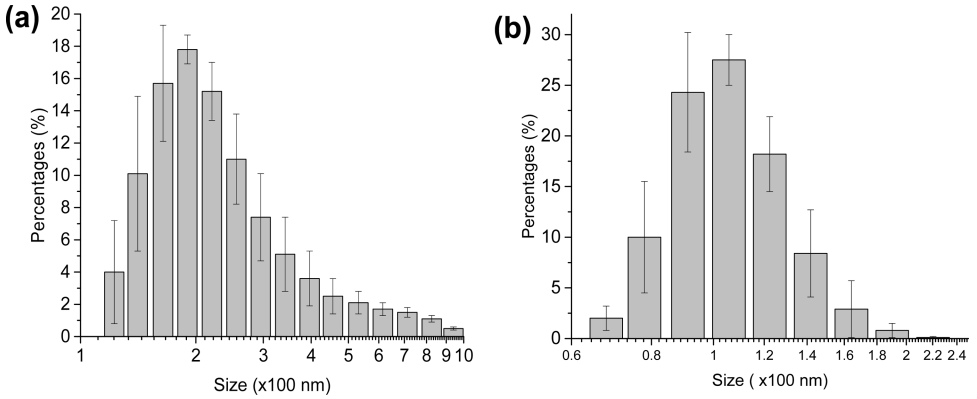

Figure 5. Particle size distribution of as-synthesized ESNP: (a) in DI water and (b) in DI water with a presence of 10% PAANa.

had good stability, while a greater deposition of ESNP with clear water was observed without PAANa.

Figure 5 shows particle size distributions of as-synthesized ESNP in DI water with the absence and presence of PAANa, which reveals the effect of PAANa on dispersion states of ESNP in aqueous solutions. As shown in Figure 5(a) from the dynamic light scattering (DLS) measurement, the number mean diameter of ESNP agglomerates in DI water was approximately 250 nm with a wide range size distribution between 100 and 1000 nm. However, the addition of PAANa leads to good dispersion of ESNP in water. The agglomerate size and distribution of ESNP in the presence of PAANa has been reduced and were in the range of 60−200 nm with a number mean diameter of approximately 95 nm as shown in Figure 5(b).

However, it is understood that the dispersion observed in the solution will not remain exactly the same in the SPI resin as it will be a function of the chemistries of the resin and the ESNP. In our case, because both the ESNP and the resin are compatible with water and are processed in water, the dispersion may not change much.

Effect of ESNP on SPI Resin Sheets. ATR-FTIR spectra of SPI sheets and SPI-ESNP5 and SPI-ESNP10 nanocomposite sheets (Figure S4, Supporting Information) showed a small absorption band at 873 cm^{-1} that can be assigned to the CO_3^{2-} ions of ESNP in the SPI-ESNP5 sheets. The intensity of the band at 873 cm^{-1} increased as the content of ESNP increased, which revealed the formation of calcite crystal in the SPI sheets. However, the presence of ESNP in SPI did not change the protein conformation as the amide I band position at 1623 cm^{-1} related to β-sheet structures and the amide II band position at 1530 cm^{-1} was the same when compared to SPI sheets.

Table 3 shows the moisture content (MC) of SPI sheets as a function of ESNP content. As shown in Table 3, the effect of ESNP on MC of nanocomposites was not significant (p-value <0.05) as compared to SPI sheets (without ESNP). The MC values vary in composites in the range of 9−10% after conditioning the specimens at 65% RH and 21 °C.

Table 3. Moisture Content (MC) of SPI Sheets as a Function of ESNP Content[a]

ESNP contents	0 wt %	3 wt %	5 wt %	10 wt %
MC (%)	$9.8^{a} \pm 0.2^{ab}$	9.5 ± 0.5^{ab}	9.2 ± 0.3^{a}	9.9 ± 0.2^{b}

[a]Means not connected by the same letters are significantly different at 95% confidence level through the Tukey−Kramer HSD test.

Figure 6 shows the effect of the ESNP addition on the tensile properties of SPI sheets. Typical stress−strain plots of SPI sheets and SPI-ESNP nanocomposite sheets obtained from the tensile test are shown in Figure 6(a), and the variations in tensile properties as a function of ESNP content are shown in Figure 6(b−d). As shown in Figure 6(b−d), the Young's modulus and tensile strength of SPI sheets increased with a decrease in fracture strain at 3 and 5 wt % ESNP loading. The Young's modulus and tensile strength of the SPI/ESNP nanocomposite sheets improved with a maximum enhancement of 56% (from 675 to 1055 MPa) and 25% (from 22.6 to 28.3 MPa), respectively. Statistical analysis based on one-way ANOVA revealed that the differences in tensile strength were significant (F-ratio ∼8.2 and p-value <0.05). Tukey−Kramer all pairs HSD tests revealed that SPI and SPI-ESNP3 tensile strength values are in different groups, while there is no significant difference between SPI-ESNP3 and SPI-ESNP5 sheets. However, in case of Young's modulus, a significant difference was observed among SPI, SPI-ESNP3, and SPI-ESNP5 sheets (F-ratio ∼23.0 and p-value ≪ 0.05). Fracture strain dropped by 55% (from 24.8% to 11.2%) at 5 wt % ESNP loading in comparison to the SPI sheets. However, a substantial drop in Young's modulus and tensile strength was observed at 10 wt % ESNP loading, while fracture strain increased again.

Typical TEM images presented in Figure 7 show the distribution of 3 and 10 wt % ESNP in SPI resin sheets. As shown in Figure 7(a), a better dispersion of 3 wt % ESNP in SPI resin provided more sites to facilitate polymer−nanoparticle interaction at the interface because of higher interaction and tortuosity of the resin molecules. Both of these factors lead to the improvement in tensile strength and Young's modulus through a more efficient stress transfer mechanism.[22] However, more aggregates were observed with a higher loading (10%) of ESNP in SPI resin as shown in Figure 7(b). The interparticle distance was decreased due to higher loading that causes flocculation of ESNP after mixing. Due to poor dispersion, as evident from Figure 7(b), ESNP remains as small agglomerates in the resin blends that act as stress concentrators in composites. Early shear slippage of individual particles within these bundles may occur, which results in decreased strength and modulus.[22] The presence of PAANa that was increased in SPI sheets with an increase in ESNP might have a negative effect as it acts as plasticizer and hence increased the fracture strain with a decrease in Young's modulus and tensile strength at 10 wt % loading.

dx.doi.org/10.1021/sc5003193 | ACS Sustainable Chem. Eng. 2014, 2, 2329−2337

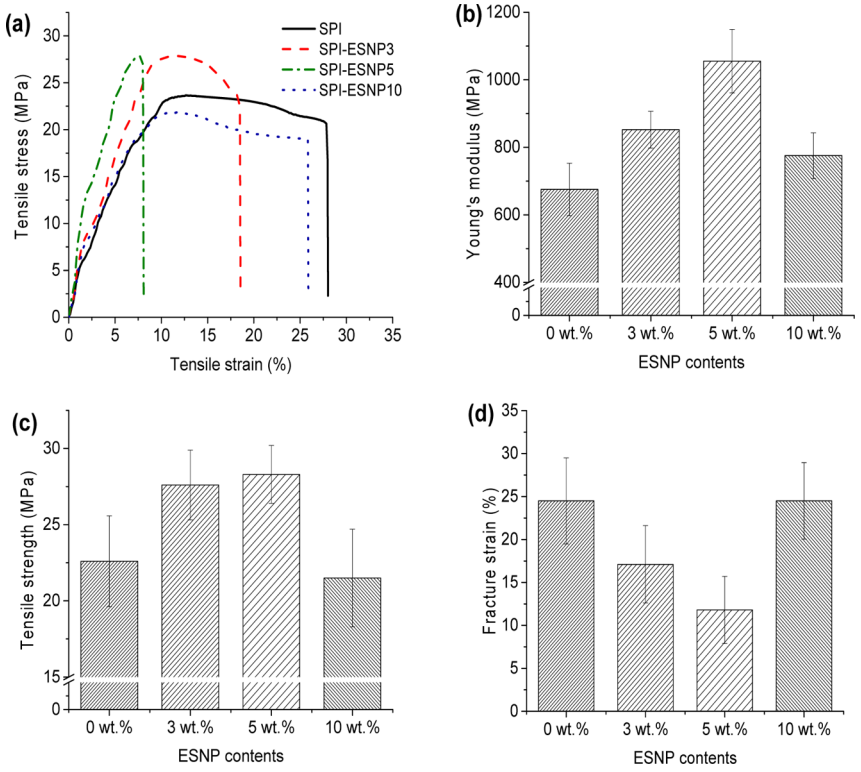

Figure 6. Effect of ESNP addition on tensile properties of SPI sheets: (a) representative stress−strain curve for SPI sheets and SPI-ESNP nanocomposite sheets, (b) Young's modulus, (c) tensile strength, and (d) fracture strain of SPI sheets and SPI-ESNP nanocomposite sheets.

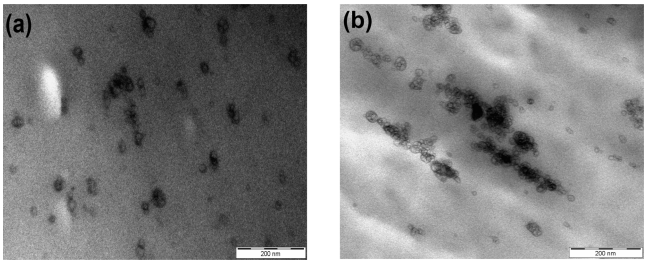

Figure 7. TEM images of 3 and 10 wt % ESNP distribution in SPI resin.

In order to investigate the fracture behavior, the surfaces of SPI sheets and 5 wt % ESNP-modified SPI composites after the tensile test were examined using SEM. SEM micrographs of fracture surfaces from (a) SPI sheets and (b) SPI-ESNP5 nanocomposite sheets are presented in Figure 8. A nearly featureless fracture surface is observed in the SPI sheet specimen as shown in Figure 8(a). The surface had less interruption of failure propagation after initiation. Figure 8(b) is the micrograph of fracture surfaces of SPI-ESNP5 specimens that show a greater degree of roughness. The rougher surface can be attributed to greater interruption of failure propagation due to the presence of ESNP.[22]

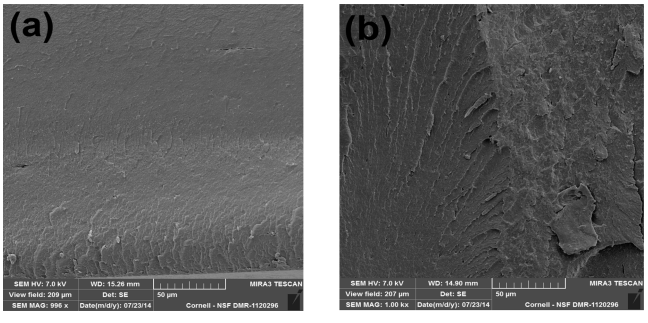

Figure 8. SEM micrographs of fracture surfaces from (a) SPI sheets and (b) SPI-ESNP5 nanocomposite sheets.

While SEM observation could not provide enough information about the distribution of ESNP in the fracture surfaces of SPI resin sheets, EDS point and mapping analysis of the fracture surface of SPI sheets and SPI-ESNP5 nanocomposite sheets was performed to confirm the presence and distribution of ESNP in the fracture surfaces of SPI sheets and SPI-ESNP nanocomposite sheets. These are shown in Figure 9. EDS point and mapping analysis of SPI sheets as a reference, shown in Figure 9(a), does not indicate any Ca element, whereas EDS point analysis of the SPI-ESNP nanocomposite sheet (Figure 9b) shows the presence of a Ca element, confirming the presence of ESNP embedded in the resin. The gold and palladium signals observed in both SPI and SPI-ESNP sheets are caused by the sputtering used for SEM analysis.

XRD patterns of SPI and SPI-ESNP5 sheets (Figure S5, Supporting Information) indicated no observable change in crystallization of protein due to the presence of ESNP. A crystallization peak simply due to the physical presence of ESNP was observed in the SPI-ESNP5 sheets as ESNP was highly crystallized. The XRD patterns reveal that the mechanical properties are not influenced from the crystallization of protein but rather by ESNP loading.

The weight loss below 150 °C in the TGA and DTGA thermograms of SPI sheets and SPI-ESNP nanocomposite sheets (Figure S6, Supporting Information) is typically attributed to the evaporation of water. Plasticizer evaporation and soy polypeptide decomposition into small molecules

dx.doi.org/10.1021/sc5003193 | ACS Sustainable Chem. Eng. 2014, 2, 2329−2337

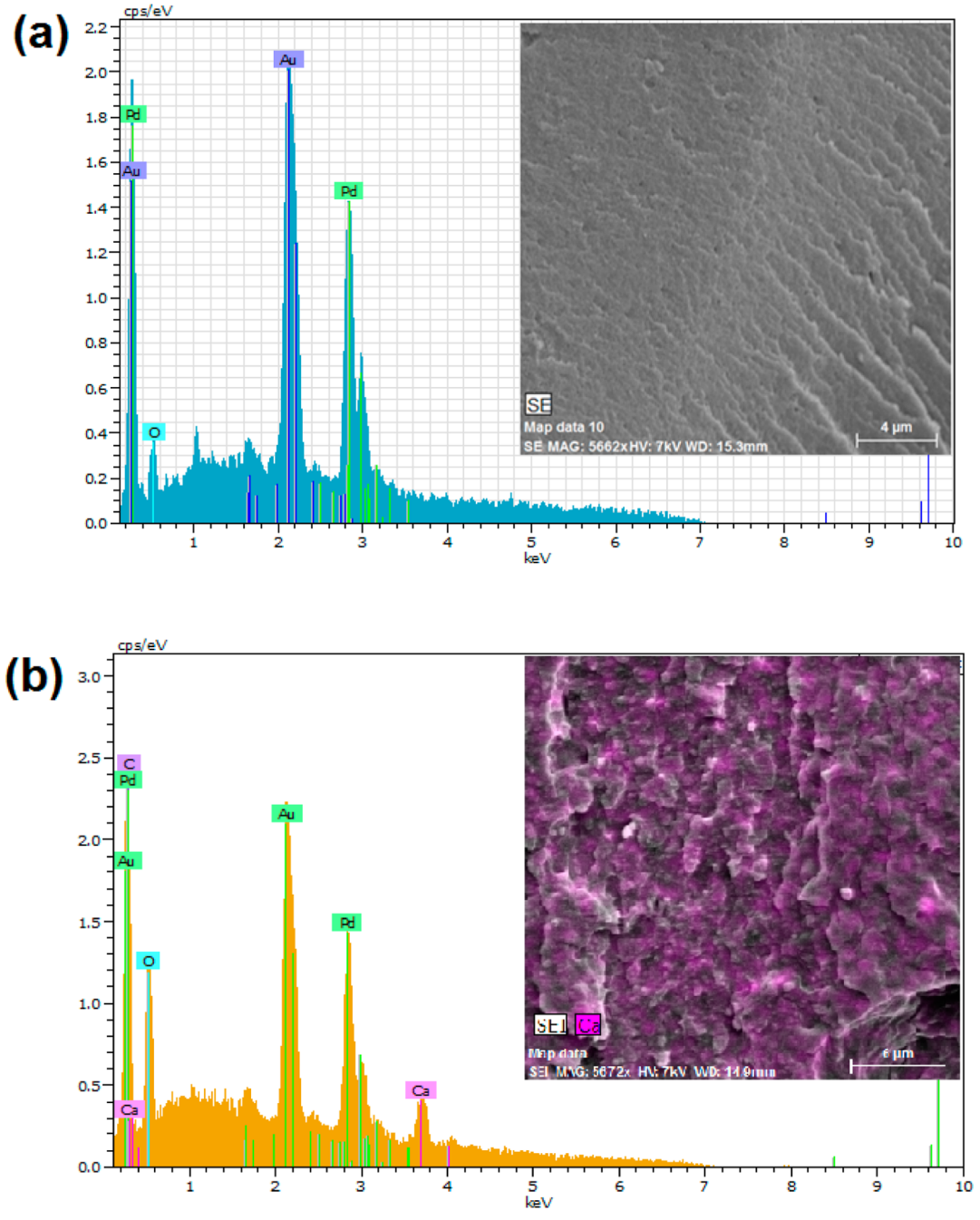

Figure 9. EDS spectrum showing point analysis with Ca elemental mapping (inset) of the fracture surfaces of (a) SPI sheets and (b) SPI-ESNP5 nanocomposite sheets.

occurred between 200 and 300 °C. The complete carbonization of soy protein occurred from 450 to 600 °C. ESNP in SPI started to decompose at 650 °C, and complete calcinations occurred after 800 °C, as similarly obtained in Figure S2 of the Supporting Information. Degradation onset temperature and residual mass of nanocomposite sheets were measured directly from the TGA thermograms, while maximum degradation temperature was measured from the DTGA thermograms. The degradation onset temperature corresponds to the inflection point of TGA thermograms. Residual mass is the yield after heating at 600 °C from TGA thermograms, and maximum degradation temperature refers to the point of maximum weight loss obtained from DTGA thermograms. As shown in Figure S6(b) of the Supporting Information, the peak of derivative weight change (maximum degradation temperature) occurred at a higher temperature for nanocomposites compared to SPI specimens without ESNP. However, the maximum degradation temperature was observed the highest for nanocomposites with 3% ESNP loading. However, with higher ESNP loading, it was observed at slightly lower temperature that might be due to the presence of higher loading of PAANa. Table 4 shows the degradation onset temperature, residual mass, and maximum degradation temperature of SPI sheets and SPI-ESNP nanocomposite sheets. Compared to the SPI sheet specimens, TGA thermograms of SPI-ESNP nanocomposite sheets shifted to a higher degradation onset temperature as well as the residual mass. The residual contents of nanocomposites at 600 °C were significantly higher than the SPI sheet due to the presence of

dx.doi.org/10.1021/sc5003193 | ACS Sustainable Chem. Eng. 2014, 2, 2329−2337

Table 4. Initial Degradation Temperature, Residual Yield, and Maximum Degradation Temperature of SPI-ESNP Nanocomposite Sheets

composition	initial degradation temp (°C)	residual yield @ 600 °C	maximum degradation temp (°C)
SPI	232.3 ± 2.8	23.7 ± 1.8	314.8 ± 2.2
SPI-ESNP3	247.7 ± 3.2	26.3 ± 1.1	322.4 ± 2.9
SPI-ESNP5	246.2 ± 2.6	28.4 ± 0.5	318.2 ± 2.1
SPI-ESNP10	243.7 ± 2.9	31.5 ± 0.9	317.5 ± 3.0

ESNP in SPI. The nanocomposites started to degrade, reached the peak, and finished degrading at higher temperatures with higher residual yield compared to SPI sheets. It was also observed that a particular conversion corresponded to a higher temperature for nanocomposites, indicating delayed degradation and increased thermal stability.

CONCLUSIONS

This study introduces a "green" route of developing very inexpensive and sustainable "bioderived" SPI-ESNP nanocomposites from soybean and egg byproducts. Eggshell nanopowder (ESNP), obtained by ball milling and ultrasonication, has been used successfully as nanofiller in biobased resin due to its high crystallinity, surface area, thermal degradation temperature, and stiffness to improve the functional properties of soy protein-based green composites. Good dispersion of ESNP was achieved by using the minimum amount of PAANa dispersant to utilize the potential of ESNP in composites. Investigation of ESNP loading in SPI sheets revealed an optimum ESNP content of 5% in SPI, which resulted in the best mechanical and thermal properties of SPI sheets under the current experimental conditions. However, the addition of 10% ESNP in SPI sheets showed decreased properties due to higher agglomerations and PAANa loading. In summary, this paper explores the utilization of free and/or inexpensive byproducts from food industries as a sustainable and "green" biobased advanced resin to replace conventional petroleum-derived resins in fiber-reinforced composites.

ASSOCIATED CONTENT

Supporting Information

ATR-FTIR spectra of ESNP. TGA and DTGA thermogams of ESNP. Optical images of dispersion state of ESNP in SPI sheets. ATR-FTIR spectra, XRD patterns, TGA, and DTGA thermograms of SPI and SPI-ESNP sheets. This material is available free of charge via the Internet at http://pubs.acs.org.

AUTHOR INFORMATION

Corresponding Author

*Tel.: (1) 607 255 1875. E-mail: ann2@cornell.edu.

Notes

The authors declare no competing financial interest.

ACKNOWLEDGMENTS

The authors acknowledge NSF-CREST (Grant 1137681) for funding this work. The authors also acknowledge Cornell Center for materials research facilities supported by NSF (Award DMR-1120296).

REFERENCES

(1) Chabba, S.; Matthews, G.; Netravali, A. Green" composites using cross-linked soy flour and flax yarns. *Green Chem.* **2005**, *7*, 576−581.
(2) Lodha, P.; Netravali, A. N. Characterization of stearic acid modified soy protein isolate resin and ramie fiber reinforced 'green' composites. *Compos. Sci. Technol.* **2005**, *65*, 1211−1225.
(3) Huang, X.; Netravali, A. N. Characterization of nano-clay reinforced phytagel-modified soy protein concentrate resin. *Biomacromolecules* **2006**, *7*, 2783−2789.
(4) Kim, J. T.; Netravali, A. N. Development of aligned-hemp yarn-reinforced green composites with soy protein resin: Effect of pH on mechanical and interfacial properties. *Compos. Sci. Technol.* **2011**, *71*, 541−547.
(5) Kim, J. T.; Netravali, A. N. Mercerization of sisal fibers: Effect of tension on mechanical properties of sisal fiber and fiber-reinforced composites. *Composites, Part A* **2010**, *41*, 1245−1252.
(6) Huang, X.; Netravali, A. Characterization of flax fiber reinforced soy protein resin based green composites modified with nano-clay particles. *Compos. Sci. Technol.* **2007**, *67*, 2005−2014.
(7) Huang, X.; Netravali, A. Biodegradable green composites made using bamboo micro/nano-fibrils and chemically modified soy protein resin. *Compos. Sci. Technol.* **2009**, *69*, 1009−1015.
(8) Dastidar, T. G.; Netravali, A. N. A soy flour based thermoset resin without the use of any external crosslinker. *Green Chem.* **2013**, *15*, 3243−3251.
(9) Hassan, T. A.; Rangari, V. K.; Rana, R. K.; Jeelani, S. Sonochemical effect on size reduction of $CaCO_3$ nanoparticles derived from waste eggshells. *Ultrason. Sonochem.* **2013**, *20*, 1308−1315.
(10) Tsai, W.; Yang, J.; Lai, C.; Cheng, Y.; Lin, C.; Yeh, C. Characterization and adsorption properties of eggshells and eggshell membrane. *Bioresour. Technol.* **2006**, *97*, 488−493.
(11) Yoo, S.; Hsieh, J. S.; Zou, P.; Kokoszka, J. Utilization of calcium carbonate particles from eggshell waste as coating pigments for ink-jet printing paper. *Bioresour. Technol.* **2009**, *100*, 6416−6421.
(12) Schaafsma, A.; Beelen, G. M. Eggshell powder, a comparable or better source of calcium than purified calcium carbonate: Piglet studies. *J. Sci. Food Agric.* **1999**, *79*, 1596−1600.
(13) Schaafsma, A.; Pakan, I.; Hofstede, G.; Muskiet, F.; Van Der Veer, E.; De Vries, P. Mineral, amino acid, and hormonal composition of chicken eggshell powder and the evaluation of its use in human nutrition. *Poult. Sci.* **2000**, *79*, 1833−1838.
(14) Zheng, W.; Li, X.; Yang, Q.; Zeng, G.; Shen, X.; Zhang, Y.; Liu, J. Adsorption of Cd (II) and Cu (II) from aqueous solution by carbonate hydroxylapatite derived from eggshell waste. *J. Hazard. Mater.* **2007**, *147*, 534−539.
(15) Tsai, W.-T.; Hsien, K.-J.; Hsu, H.-C.; Lin, C.-M.; Lin, K.-Y.; Chiu, C.-H. Utilization of ground eggshell waste as an adsorbent for the removal of dyes from aqueous solution. *Bioresour. Technol.* **2008**, *99*, 1623−1629.
(16) Park, J.-W.; Bae, S.-R.; Suh, J.-Y.; Lee, D.-H.; Kim, S.-H.; Kim, H.; Lee, C.-S. Evaluation of bone healing with eggshell-derived bone graft substitutes in rat calvaria: A pilot study. *J. Biomed. Mater. Res., Part A* **2008**, *87*, 203−214.
(17) Toro, P.; Quijada, R.; Yazdani-Pedram, M.; Arias, J. L. Eggshell, a new bio-filler for polypropylene composites. *Mater. Lett.* **2007**, *61*, 4347−4350.
(18) Lin, Z.; Zhang, Z.; Mai, K. Preparation and properties of eggshell/β-polypropylene bio-composites. *J. Appl. Polym. Sci.* **2012**, *125*, 61−66.
(19) Bootklad, M.; Kaewtatip, K. Biodegradation of thermoplastic starch/eggshell powder composites. *Carbohydr. Polym.* **2013**, *97*, 315−320.
(20) Sisakht Mohsen, R.; Saied, N. K.; Ali, Z.; Hosein, E. M.; Hasan, P. Theoretical and experimental determination of tensile properties of nanosized and micron-sized $CaCO_3$/PA66 composites. *Polym. Compos.* **2009**, *30*, 274−280.
(21) Ciprari, D.; Jacob, K.; Tannenbaum, R. Characterization of polymer nanocomposite interphase and its impact on mechanical properties. *Macromolecules* **2006**, *39*, 6565−6573.

(22) Rahman, M.; Zainuddin, S.; Hosur, M.; Malone, J.; Salam, M.; Kumar, A.; Jeelani, S. Improvements in mechanical and thermo-mechanical properties of e-glass/epoxy composites using amino functionalized MWCNTs. *Compos. Struct.* **2012**, *94*, 2397−2406.
(23) Chan, C.-M.; Wu, J.; Li, J.-X.; Cheung, Y.-K. Polypropylene/calcium carbonate nanocomposites. *polymer* **2002**, *43*, 2981−2992.
(24) Liu, D.; Tian, H.; Jia, X.; Zhang, L. Effects of calcium carbonate polymorph on the structure and properties of soy protein-based nanocomposites. *Macromol. Biosci.* **2008**, *8*, 401−409.
(25) Lin, Y.; Chen, H.; Chan, C.-M.; Wu, J. High impact toughness polypropylene/$CaCO_3$ nanocomposites and the toughening mechanism. *Macromolecules* **2008**, *41*, 9204−9213.
(26) Avella, M.; Errico, M. E.; Martuscelli, E. Novel PMMA/$CaCO_3$ nanocomposites abrasion resistant prepared by an in situ polymerization process. *Nano Lett.* **2001**, *1*, 213−217.
(27) Sze, A.; Erickson, D.; Ren, L.; Li, D. Zeta-potential measurement using the Smoluchowski equation and the slope of the current−time relationship in electroosmotic flow. *J. Colloid Interface Sci.* **2003**, *261*, 402−410.
(28) Rhim, J. W.; Gennadios, A.; Weller, C. L.; Cezeirat, C.; Hanna, M. A. Soy protein isolate−dialdehyde starch films. *Ind. Crops Prod.* **1998**, *8*, 195−203.
(29) Klug, H. P.; Alexander, L. E. *X-ray Diffraction Procedures: For Polycrystalline and Amorphous Materials*; 2nd ed.; Wiley Interscience: New York, 1974; Vol. *1*.
(30) Derjaguin, B. Theory of the stability of strongly charged lyophobic sols and the adhesion of strongly charged particles in solutions of electrolytes. *Acta Physicochim. USSR* **1941**, *14*, 633−662.
(31) Verwey, E. Theory of the stability of lyophobic colloids. *J. Phys. Chem.* **1947**, *51*, 631−636.
(32) Cho, K.; Chang, H.; Kil, D. S.; Kim, B.-G.; Jang, H. D. Synthesis of dispersed $CaCO_3$ nanoparticles by the ultrafine grinding. *J. Ind. Eng. Chem.* **2009**, *15*, 243−246.
(33) Kawashima, S.; Seo, J.-W. T.; Corr, D.; Hersam, M. C.; Shah, S. P. Dispersion of $CaCO_3$ nanoparticles by sonication and surfactant treatment for application in fly ash−cement systems. *Mater. Struct.* **2013**, 1−13.
(34) Ivanova, N.; Shchukin, E. Mixed adsorption of ionic and non-ionic surfactants on calcium carbonate. *Colloids Surf., A* **1993**, *76*, 109−113.
(35) Loiseau, J.; Ladaviere, C.; Suau, J.; Claverie, J. Dispersion of calcite by poly (sodium acrylate) prepared by reversible addition−fragmentation chain transfer (RAFT) polymerization. *Polymer* **2005**, *46*, 8565−8572.
(36) Mijan, M. A.; Kim, D. H.; Kwak, H. S. Physicochemical properties of nanopowdered eggshell. *Int. J. Food Sci. Technol.* **2013**, 1−7.